

Comparative Study of High Voltage Spinel || Lithium Titanate Lithium-ion Batteries in Ethylene Carbonate Free Electrolytes

Killian Stokes-Rodriguez,^[a] Kaushik Jayasayee,^[a] Sidsel M. Hanetho,^[a] Jannicke Kvello,^[a] Peter P. Molesworth,^[b] Øystein Dahl,^[c] and Nils Peter Wagner^{*[a, d]}

A persistent obstacle towards the realization of high voltage cathodes is electrolyte instability where oxidation and transition metal dissolution manifest in rapid capacity failure with both issues connected to the presence of ethylene carbonate in the electrolyte. Here, alternative electrolyte co-solvents are investigated and compared, where the cyclic carbonate is replaced with sulfones ethyl methyl sulfone (EMS) and tetra methylene sulfone (TMS) and fluoroethylene carbonate (FEC). The best full cell performance was observed for cells cycled in a FEC/EMC (3/7) and FEC/EMC (1/1) electrolytes which exhibited 84–85% capacity retention after 500 cycles. TMS/EMC (3/7), was determined to be the best performing sulfone electrolyte and

maintained 71% capacity after 500 cycles. Post-mortem XPS analysis indicated different film forming mechanisms for the respective co-solvent. A thicker cathode electrolyte interphase (CEI) on the LNMO was observed for the FEC containing electrolytes (relative to when TMS was used as the co-solvent) indicating more effective passivation of the reactive cathode surface which correlated well with the enhanced cycling stability observed. For LTO, more evidence of transition metal migration and a thicker solid electrolyte interphase (SEI) layer was observed for the sulfone electrolyte suggesting more parasitic anode-electrolyte interactions and an inability to mitigate Mn²⁺/Ni²⁺ crosstalk.

Introduction

Accounting for approximately 50% of the cell weight, the choice of electrodes is crucial in maximizing the energy density of a lithium-ion battery (LIB).^[1] Due to high operating potentials (4.7 V vs Li/Li⁺), high energy density and the absence of cobalt within its structure spinel LNMO has emerged as one of the most promising cathode materials of the future.^[2–4] However, the high operating voltages come with a caveat, where the cathode is prone to parasitic side reactions with the electrolyte, namely electrolyte decomposition and transition metal migration. Conventional electrolytes are non-aqueous solvents, typically consisting of a combination of linear carbonates

(dimethyl carbonate (DMC), diethyl carbonate (DEC), etc.) and cyclic carbonates (propylene carbonate (PC), ethylene carbonate (EC), etc.) with limited electrochemical stability above 4.3 V.^[5,6] Therefore, when operating above these voltages, oxidation of the electrolyte components will readily occur, manifesting in loss of cyclable lithium, increasing the internal cell resistance and resulting in rapid capacity fade.

EC remains among the most used co-solvents, its presence in the electrolyte matrix has been shown to have debilitating effects when cycling at high voltages. While EC is known to be among the most stable molecules against oxidation, due to its high dielectric constant it will still coordinate strongly with the PF₆⁻, from the lithium salt. Therefore, during charging EC will quickly reach the reactive cathode surface and undergo preferential oxidation. The subsequent radical cation (EC^{•+}) generated following a one electrode oxidation reaction has been shown to form CO, CO₂ and highly reactive cation radicals which will partake in additional unwanted side reactions within the cells.^[7–9]

Crosstalk describes the interactions occurring between the positive and negative electrodes. Operating at higher voltages has shown a tendency towards dissolution of transition metals (Mn²⁺ and Ni²⁺) at the cathode followed by subsequent migration to, and deposition at the anode. A previous study by Klein et al. linked the rapid failure of high voltage (<4.5 V) NCM523 || graphite cells to severe alteration of the anode surface due to migration of TMs from the cathode which subsequently induced the formation of Li metal dendrites.^[10,11] A follow-up study utilizing EC-free electrolytes, again in NCM523 || graphite cells, revealed significantly less transition metal (TM) migration (and dendrite formation) compared to

[a] K. Stokes-Rodriguez, K. Jayasayee, S. M. Hanetho, J. Kvello, N. Peter Wagner
Department of Sustainable Energy Technology, SINTEF Industry, 7491 Trondheim, Norway

[b] P. P. Molesworth
Department of Biotechnology and Nanomedicine, SINTEF Industry, 7491 Trondheim, Norway

[c] Ø. Dahl
Department of Materials and Nanotechnology, SINTEF Industry, 7491 Trondheim, Norway

[d] N. Peter Wagner
Department of Materials Science and Engineering, NTNU Norwegian University of Science and Technology, 7491 Trondheim, Norway
E-mail: nils.peter.wagner@sintef.no

Supporting information for this article is available on the WWW under
<https://doi.org/10.1002/batt.202400457>

© 2024 The Authors. *Batteries & Supercaps* published by Wiley-VCH GmbH.
This is an open access article under the terms of the Creative Commons Attribution License, which permits use, distribution and reproduction in any medium, provided the original work is properly cited.

when EC was present as a co-solvent in the electrolyte matrix. Here, a mechanism where the lack of EC facilitated an increased LiPF₆ degradation into species which can effectively trap TMs and subsequently suppress dendrite formation was proposed.^[12]

Sulfones are flame retardant solvents with a high dielectric constant and high oxidation stability. They show promise as an electrolyte component for high voltage Li ion battery applications due to their high electrochemical stability beyond >5 V.^[6,13] Sulfones are less prone to electronic polarization and typically unreactive towards the surface of high voltage cathodes, because of the high oxidation state of the center atom. The limiting factor when using these electrolytes is their high viscosity which typically implies low conductivity. An effective route to utilize their desirable properties can be achieved by pairing with a more conductive, less viscous co-solvent. The addition of alkyl carbonates to sulfones has been shown to reduce viscosity and enhances ionic conductivity.^[14] A study by Xue et al demonstrated that EMS can confer its high voltage stability to DMC when used as a co-solvent for cycling of LNMO full cells.^[15] Similar findings have been observed when adding sulfone co-solvents, such as trifluoromethyl sulfone, to EC and DMC.^[16] An additional persisting issue with utilizing sulfones remains in its incompatibility with the graphite anode. Here, it will be reduced to an insoluble dimer which results in parasitic reactions on the graphite surface, forming an unstable solid electrolyte interphase (SEI).^[13,17] Therefore, sulfone-based electrolytes may be best suited when paired with a high voltage anode material, such as LTO, whereby, it may be an effective electrolyte for high-power LIBs.

Due to their film-forming abilities on the anode side, in particular for the stable cycling of silicon-containing anodes, fluorinated carbonates have attracted extensive research attention as electrolyte additives.^[18–20] To date, effective anode stabilization has been demonstrated by difluoroethylene carbonate (DFEC), trifluoropropylene carbonate (TFPC), and Methyl 2,2,2-trifluoroethyl carbonate (F-EMC) with the most prevalent fluorinated carbonate investigated being fluoroethylene carbonate (FEC).^[21–26] While primarily used in additive quantities, less commonplace are studies where FEC is used as an electrolyte solvent or co-solvent. Fluorinated carbonate electrolytes possess desirable properties such as increased oxidation stability (relative to EC) and reduced flammability. Such factors make them, in theory, a suitable electrolyte for high voltage applications. However, there remains a lack of a consensus on FEC's effectiveness in the stabilization of LNMO and other high voltage cathodes with reports published showing it impart neutral/negative or positive effects in stabilizing the cathode interface.^[19,27–31] Yet, such reports where the presence of FEC has been deemed inconsequential or hindering have also featured EC in their respective electrolyte matrices. Therefore, a systematic characterization of FEC as a co-solvent substitute, in lieu of EC, is necessary before dismissing its potential for high voltage lithium-ion battery applications. This is especially important for an electrolyte component that is well known to be effective in stabilizing the anode.

In this study, the performance of EC-free electrolytes is elucidated for LNMO||LTO cells at both room and at elevated temperatures. Three co-solvents were analyzed where TMS, EMS and FEC are combined with EMC in different volume (or weight) ratios, 1/1 and 3/7 and their suitability for high voltage Li-ion battery cycling was investigated by testing in LNMO || LTO full-cells. While half-cell testing is useful in the validation of the electrode of interest, the stable and theoretically infinite supply of Li ions disregards any depletion of the Li inventory (e.g. during the formation of electrode interphases). Hence, it becomes difficult to correlate the influence of the electrolyte to a true electrochemical cell scenario as the electrolyte will have implications on both electrodes while in an environment where the Li supply is limited. LTO, as a negative electrode is already used in portable electronics and in stationary storage applications when paired with LFP, LMO, LCO and LMPO. However, anode active materials comprised of titanium have some drawbacks with regards to reactivity towards conventional electrolytes which leads to the formation of gasses (CO₂, CO, H₂) during cycling.^[32] LTO also possess lower specific capacity (and hence lower energy density), due to its high delithiation potential, relative to graphite. Nevertheless, LTO has advantages over graphite whereby its higher operating potentials limits the deposition of metallic lithium during operation, thus ensuring cell safety.^[33] In this investigation, LTO was employed as the anode on account of its electrochemical stability and suitability as a high voltage anode. Hence, differences in electrochemical behavior can be better correlated to influences coming from the different electrolytes tested and ascribed to the resulting SEI and cathode electrolyte interphase (CEI) formed. The electrodes cycled in the EC-free electrolytes were comprehensively analyzed and contrasted, in the absence of any electrolyte additives, in terms of their high voltage stabilities, through linear sweep voltammetry, galvanostatic cycling stability and by utilizing post-mortem XPS analysis to characterize the consequential SEIs (LTO) and CEIs (LNMO) formed after extended cycling.

Experimental Section

Electrolyte Preparation

Electrolyte preparation was carried out in an Ar filled glovebox (MBraun O₂ and H₂O levels <0.1 ppm). The ethylene carbonate free electrolytes investigated in this study consisted of a blend of a high permittivity solvent together with a low viscosity solvent in both 1:1 and 3:7 volume ratio. The high permittivity solvents were fluoroethylene carbonate (FEC, Sigma Aldrich ≥ 99%, acid <200 ppm, anhydrous), ethylmethyl sulfone (EMS, VWR, >98%) and tetramethylene sulfone also called Sulfolane (TMS, VWR, >99%). The employed low viscosity solvent in this study was the linear ethyl methyl carbonate (EMC, employed as premixed 1 M LiPF₆ solution, Sigma Aldrich, battery grade, 99,99%). All high permittivity solvents were dried over molecular sieves (3 Å Sigma Aldrich) for 48 h before they were filtered and blended with the 1 M LiPF₆ in EMC solution in 1:1 and 3:7 volume ratio. In a final step additional LiPF₆ (Sigma Aldrich, battery grade, ≥ 99.99%) was added to obtain a molarity of 1 M. As the salt concentration throughout the experimental matrix was fixed (1 M), the following

notation will be used: (high permittivity solvent (FEC, TMS or EMS))/EMC v/v (1/1 or 3/7).

Electrode Fabrication and Cell Assembly

Positive electrode laminates were processed by homogenizing 90 wt.% commercial LNMO powder (Topsoe, Denmark), 5 wt.% carbon black (Imerys C-nergy Super C 65) and 5 wt.% PVDF (KYNAR HSV 900) dissolved in n N-methyl-2-pyrrolidone (NMP) using a Retsch MM400 shaker mill. First the carbon black was dispersed in a binder solution at a frequency of 25 Hz for 5 min. In a second step, the active material and additional solvent was added, and the slurry was homogenized at a frequency of 25 Hz for 30 min. The electrode slurry was cast on battery grade Al foil (20 µm) and dried at 80°C for 3 h. To ensure good contact within the electrode laminate, it was roll pressed to 90% of its dry thickness (corresponding to geometric densities in the range of 1.6 – 1.7 gcm⁻²). Circular electrodes ($\varnothing = 16$ mm) were cut, and vacuum dried at 120°C for 12 h prior to being transferred into an Ar filled glove box. The LNMO cathodes had a typical active loading of 8–9 mgcm⁻² translating to an areal capacity of ~1.1–1.3 mAhcm⁻² based on a specific capacity of 147 mAh/g. Cathode limited full cells were assembled using oversized Li₄Ti₅O₁₂ (LTO, 18 mm \varnothing , 2 mAhcm⁻², Custom Cells, Germany) negative electrodes. All full cell tests were carried out in CR 2016 stainless steel coin cells (Hohsen) using 40 µL of the electrolytes defined above and a Celgard 2400 separator ($\varnothing = 19$ mm).

Electrochemical Assessment

The ionic conductivity of all electrolytes was assessed by potentiostatic electrochemical impedance spectroscopy (PEIS) using a TSC measuring cell type with Pt electrodes in combination with a Microcell HC setup (RHD instruments GmbH & Co. KG) on an Autolab PGSTAT204 potentiostat (Metrohm). Prior to the measurements the cell constant was determined at 20°C using a 0.1 M KCl standard solution. The PEIS measurements were performed in a frequency range of 400 kHz to 100 Hz with an AC voltage amplitude of 50 mV. Measurements were performed between –10°C and 50°C in 10°C intervals (Peltier T control accuracy 0.1°C). The data was fitted to a resistor and constant phase element in series.

The anodic stability of all electrolytes was probed by galvanostatic overcharge experiments in LNMO||LTO (E LTO~1.55 V vs. Li/Li⁺) cells at a charge rate of C/5 at 20°C. Certain samples were further tested at 45°C as well as by linear sweep voltammetry (LSV). LSV analyses were performed in three electrode PAT-type cells (EL Cell, Germany) with Li counter and reference electrodes. To increase the surface area and mimic a realistic system C coated Al foil was used as working electrode. LSV scans were recorded from OCV to 6 V vs. Li/Li⁺ with a scan rate of 1 mVs⁻¹ on a Biologic VMP300 potentiostat at room temperature and 45°C.

The cycle-life of LNMO||LTO cells with the 6 different electrolyte compositions was assessed by galvanostatic cycling for 500 cycles at 20°C on a LANDT CTA2001A battery cycler. The cell formation was done by three slow cycles at C/10 between 3.4 and 2.1 V. Thereafter the cells were cycled for 5 cycles at C/2 in cc–cv mode (cv until the current dropped to a C/10 equivalent). Then the discharge rate was increased to 1 C. Self-discharge experiments were carried out for selected samples by storing them at 100% SOC for 20 h and 168 h prior to discharge. Furthermore, the power capability was estimated by discharging selected cells at increasing rate from 1 C to 5 C and monitoring the cell voltage. The asymmetric rate test was conducted using the same charging

protocol as in the galvanostatic cycling, above, (C/2 in CC–CV mode). Following each discharge rate analyzed, the cells were discharged again at C/5 to ensure complete discharge after each cycle.

Physicochemical Characterization

XPS analysis was performed on the electrodes extracted from LNMO||LTO cells cycled with 1 M LiPF₆ in TMS/EMC 3/7 or FEC/EMC 3/7 after 50 cycles at room temperature. Prior to analysis the cells were opened in an Ar filled glove box, rinsed several times with DMC, mounted on carbon tape on a sample stub, and placed in the inert transfer arm. The transfer arm was mounted on the XPS and vented with Ar gas before the sample was transferred.

XPS was measured on Kratos Axis Ultra, using monochromatized Al K-alpha radiation with hybrid lens setting and a slot aperture (measurement area approx. 300x700 µm²). The F 1s, C 1s, and S 2p region were measured first before the remaining detail and survey spectra were measured. Detail spectra used 20 eV or 40 eV pass energy and survey spectra were measured with 160 eV pass energy. CasaXPS software was used for the data analysis. The LNMO electrodes showed differential charging during the initial stages of the measurements, causing transitions related to PVDF and CEI to shift by 0.3 eV to higher binding energies compared to the C-black transition before a steady state condition was reached. Transitions related to the TMO remained constant. The LTO electrodes showed no dynamic charging effects, however, the binding energy of the C–C contribution was higher (285.7 eV) than normal, indicating charging. In order to compare the composition of the CEI and SEI layers on the LNMO and LTO electrodes the binding energies were corrected. For the LNMO electrodes the CF₂ component to the C 1s spectrum was used as the binding energy reference (290.7 eV), and the C–C contribution (284.8 eV) was used for LTO electrodes. SEM EDS was performed using a Hitachi S-3400 N on uncycled electrodes to guide the XPS observations.

Results and Discussion

The physical data of all solvents used in this study are shown in Table 1. As a comparison the most used aprotic high dielectric LIB electrolyte solvents ethylene carbonate and propylene carbonate are shown for comparison.

Most high permittivity solvents have both a high melting point and a high viscosity, where propylene carbonate is an exception to the rule on the former property. TMS stands out with a very high viscosity in comparison to the other solvents shown, however Abouimrane and Amine showed it to offer excellent anodic stability and a lower flammability compared to ethylene carbonate-based electrolytes.^[39] To ensure sufficient ionic mobility, particularly at lower temperatures, it is necessary to blend TMS with a low melting, low viscosity component. In this study, ethyl methyl carbonate (EMC) was employed as the low viscosity component.

Potentiostatic electrical impedance spectroscopy (PEIS) was used to determine the temperature dependent ionic conductivities of the investigated electrolytes between –10 and 50°C (Figure 1). The impedance spectra in Nyquist representation and the obtained resistance values are summarized in Figure S1 and Table S1. The temperature dependence of all electrolytes is not well described by the Arrhenius equation, as the activation

Table 1. Physical properties* of the solvents used in this study and the two most commonly used high permittivity solvents ethylene and propylene carbonate.

Solvent	Abbre.	Tm /°C	Tb /°C	Dielectric constant (ϵ_r)	Viscosity /cP	Ref
Ethyl methyl carbonate	EMC	<M- > 53 ³⁴	110	2.958	0.65 ³⁵	[34, 35]
Ethyl methyl sulfone	EMS	36	240	58 ³⁶	4 (35 °C)	[36, 37]
Tetramethylene sulfone	TMS	20 ¹⁴	285	43	10.29	[14, 35]
Fluoroethylene carbonate	FEC	18	249	78.4 (23 °C)	4.10 (25 °C)	[38]
Ethylene carbonate	EC	36.5	238	90.46 (40 °C)	1.9 (40 °C)	[35]
Propylene carbonate	PC	<M- > 54.53	242	64.96	2.512	[35]

* Physical properties are cited from ref. [14, 34–38].

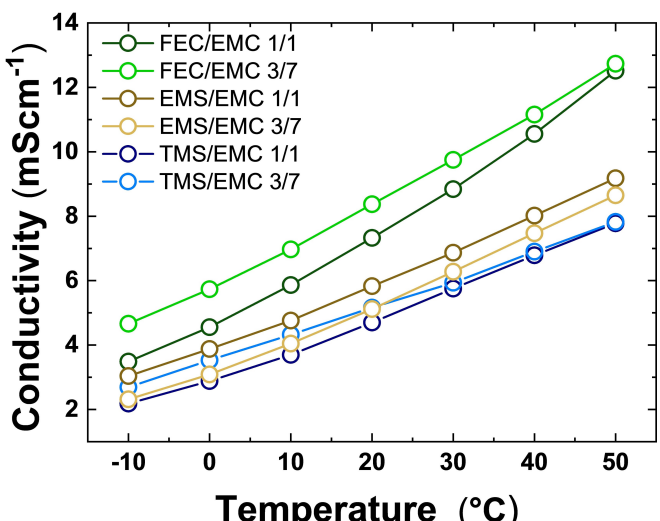


Figure 1. Ionic conductivity measurements of 1 M LiPF₆ in FEC/EMC, 1 M LiPF₆ in TMS/EMC and EMS/FEC in 1/1 and 3/7 ratios, in the temperature range from -10 °C–50 °C.

energy shows temperature dependency. Instead, all electrolytes could be reasonably fitted to the empirical Vogel-Fulcher-Tammann equation.^[40–42] The VFT fits and derived Vogel temperatures are provided in Figure S2 and Table S2, respectively. The electrolytes with FEC as a co-solvent displayed the highest conductivities which were within the typical ranges observed for LP50 and 57 electrolytes.^[43] FEC/EMC demonstrated the highest temperature dependency of the electrolytes tested, where ionic conductivity improved three-fold from -10 °C (4.5 mScm⁻¹) to 50 °C (13 mScm⁻¹). At 20 °C FEC/EMC 3/7 showed the highest conductivity at 8.4 mScm⁻¹. In contrast, the lowest ionic conductivities were observed for the TMS containing electrolytes, where the 20 °C value only reached 4.7 mScm⁻¹. Yet, the temperature dependency is lower. The low conductivities are likely due to the high viscosity of the cyclic sulfone. EMS has a similar viscosity to FEC albeit at a lower relative permittivity. Using the sulfone solvent as a co-solvent results in up to 5.8 mScm⁻¹ at 20 °C, which is an improvement in conductivity to previous studies where the sulfone is utilized as the sole electrolyte solvent.^[44]

Overcharge experiments in LNMO||LTO cells were conducted to investigate the oxidative stability of the electrolytes

at both room and high temperatures (45 °C) as shown in Figure 2. The shown incremental capacity profiles focus on the cell voltage from 3 to 4.3 V which translates to 4.5 and 5.9 V vs. Li/Li⁺. The overcharge data is shown in Figure S3. At room temperature (Figure 2a) all electrolytes exhibit promising stability up to 5.4 V vs. Li/Li⁺, with little detectable activity above the de-lithiation potential of LNMO and the onset of oxidation. The main onset of irreversible electrolyte oxidation lies lowest for the cyclic TMS based systems, shortly followed by the linear EMS/EMC and FEC/EMC in 3/7 volume ratio. Both, FEC and EMS in 1/1 volume ratio demonstrate a delayed onset at beyond 5.6 V vs. Li/Li⁺. The oxidative stabilities of the FEC/EMC 3/7 and TMS/EMC 3/7 electrolytes were also examined at 45 °C (Figure 2b). In both cases the onset of oxidation is shifted to lower potentials, with the most significant decrease observed for the FEC-based electrolyte, where the main decomposition accelerated at 5.35 V vs. Li/Li⁺. Given that small parasitic currents might go undetected during cell overcharge, linear sweep voltammetry (LSV) studies were performed on FEC/EMC (3/7) and TMS/EMC (3/7). Figure 2c and d compares the LSVs of both samples at room (20 °C) and at an elevated temperature (45 °C). For both electrolytes, minor onsets of oxidative currents begin to appear from 4.2 V vs. Li/Li⁺. However, the main difference is that the FEC based electrolyte shows elevated anodic currents onsetting at 4.9 V vs. Li/Li⁺, whilst the TMS based counterparts exhibit much lower currents below 5.3 V vs. Li/Li⁺. At higher temperatures, the oxidation onset occurs earlier, with the main anodic currents at 45 °C starting around 4.8 V vs. Li/Li⁺, making them less suitable for high voltage cathodes. Additionally, the FEC-based electrolyte, further small anodic currents occur between 4.2 and 4.5 V vs. Li/Li⁺.

To evaluate the high voltage stability and viability of the sulfone- and fluorinated carbonate-based electrolytes, full cells of LNMO vs. LTO were assembled in coin cells and underwent long term galvanostatic cycling. Cell formation was performed with three slow cycles at C/10 between 3.4 and 2.1 V. Subsequently, the cells were cycled for five cycles at C/2 in constant-current, constant-voltage (CC–CV) mode, with CV until the current dropped to a C/10 equivalent. Following this, the discharge rate was increased to 1 C while maintaining the same C/2 charge rate, within the same voltage limits. Figure 3 shows the voltage curve of all LNMO||LTO cells for the first, fifth, and tenth cycle. For all electrolytes, the voltage profile displays the

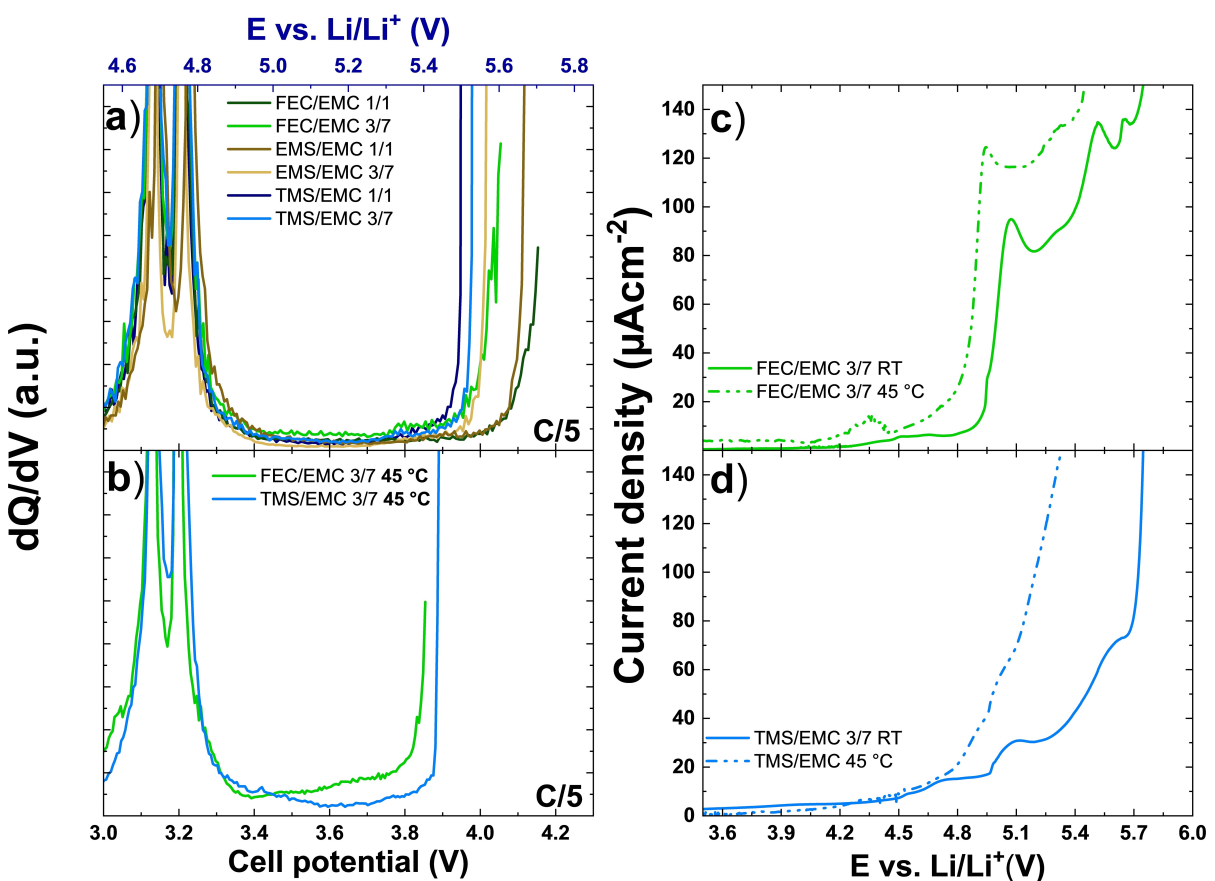


Figure 2. Derived incremental capacity plots from LNMO||LTO overcharge experiments at a) room temperature and b) 45 °C. Linear sweep voltammetry scans at room temperature and 45 °C of c) 1 M LiPF₆ in FEC/EMC 3/7 and d) 1 M LiPF₆ in TMS/EMC 3/7.

characteristic features of LNMO, with two main plateaus during charge and discharge corresponding to the Ni²⁺/Ni⁴⁺ (3.1 V vs. LTO) and Mn³⁺/Mn⁴⁺ (2.4 V vs. LTO) redox activity.^[4,45]

The TMS/EMC 1/1 electrolyte exhibited the highest first cycle coulombic efficiency at 92.8%, followed by TMS/EMC 3/7 with 91.2%. The corresponding reversible discharge capacities were 133.3 mAhg⁻¹ and 134.8 mAhg⁻¹, respectively. FEC/EMC 3/7 displayed first cycle coulombic efficiencies of 88.2% with a reversible discharge capacity of 128.1 mAhg⁻¹, while FEC/EMC 1/1 demonstrated a first cycle efficiency of 86.7% with a reversible capacity of 125.7 mAhg⁻¹. The cells cycled with FEC-containing electrolytes had the lowest initial discharge capacities in this study, with a noticeable decrease in Mn^{3+/4+} activity around 2.4 V vs. LTO, indicating Li ion consumption due to more extensive interphase formation. The reduction of FEC is reported to occur at around 1.2–1 V vs. Li/Li⁺.^[46,47] However, Yao et al. reported reduction onsets as early as 1.6 V vs. Li/Li⁺ in FEC/DEC based electrolytes, which would suggest SEI formation within the potential limits of the LTO anode used in this study.^[48] The LSV analysis (Figure 2) further suggest oxidative side reaction to occur towards the end of charge, potentially leading to the formation of a CEI based on FEC degradation products. These reactions likely involve the consumption of Li ions, explaining the higher capacity losses in the initial cycles for the FEC based electrolytes. Overall, EMS/EMC electrolytes

displayed the lowest first cycle efficiencies, with 86.6% (3/7) and 83.7% (1/1). Their first reversible capacities were 133.7 mAhg⁻¹ (EMS/EMC 3/7) and 131.1 mAhg⁻¹ (EMS/EMC 1/1), which were comparable to those observed for the TMS-based cells suggesting little Li inventory consumption during the side reactions. By the 5th and 10th cycle, all cells, except for EMS/EMC 1/1, maintained the same reversible capacities, and displayed little to no capacity fade. The voltage profiles for the EMS/EMC 1/1 cell show a clear and increasing polarization, relative to the other electrolytes, and retained only 92% of its initial capacity by the 10th cycle. Additionally, significant polarization, particularly at the 1 C discharge rate, was observed for FEC/EMC 3/7 and FEC/EMC 1/1. Despite higher conductivity values for FEC-based electrolytes, the increased cell polarization is likely due to the formation of a thicker interphase.

Figure 4 shows the electrochemical analysis data of the LNMO/LTO cells. All electrolytes underwent long term cycling for 500 cycles LNMO||LTO cells. The results and the corresponding coulombic efficiencies are shown in Figure 4 a and b respectively. In the initial cycles, the sulfone-containing electrolytes exhibited higher reversible capacities than their FEC-containing counterparts. However, the sulfone electrolytes demonstrated much quicker capacity fade, with only TMS/EMC (3/7) maintaining higher capacities than FEC/EMC by the 50th cycle. After 500 cycles, the best-performing electrolytes in terms

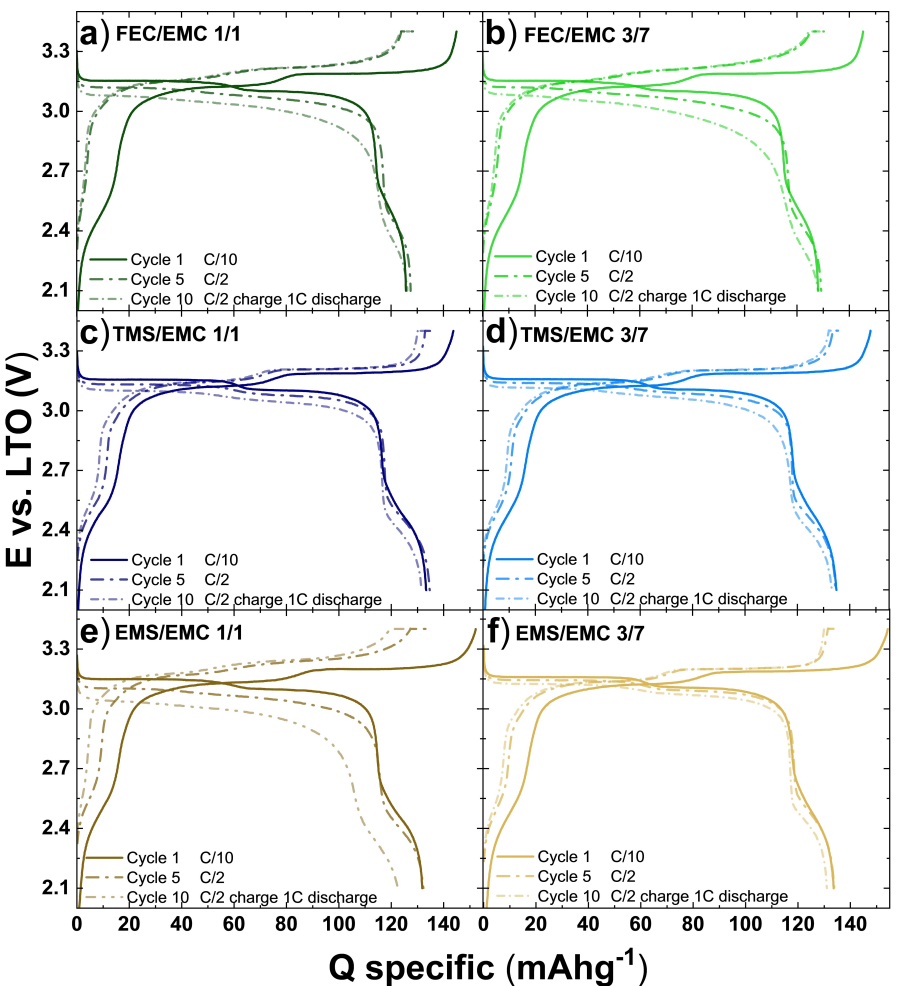


Figure 3. Voltage profile of the first, fifth and tenth cycle of LNMO//LTO cells cycled with 1 M LiPF₆ in a) FEC/EMC 1/1, b) FEC/EMC 3/7, c) TMS/EMC 1/1, d) TMS/EMC 3/7, e) EMS/EMC 1/1 and f) EMS/EMC 3/7.

of reversible discharge capacity and capacity retention were the FEC/EMC blends. These cells retained capacities of 107.1 mAhg⁻¹ (3/7) and 106.1 mAhg⁻¹ (1/1), representing 84% and 85% of their initial capacities, respectively. Conversely, the worst-performing electrolytes were TMS/EMC 1/1 and EMS/EMC 1/1. Cells cycled with EMS/EMC 1/1 exhibited rapid capacity fade over the initial 50 cycles before stabilizing at a reversible discharge capacity of 82 mAhg⁻¹, resulting in a 30% capacity loss. The cells cycled in TMS/EMC 1/1 showed a more gradual, but continuous decay, never reaching a point of stabilization and retaining only 66 mAhg⁻¹ after 500 cycles. This suggests an inability to form a stable passivation layer on the electrodes with this electrolyte. Furthermore, it is suggested that the poor performance of both sulfone based electrolytes in 1/1 ratio is related to their high viscosity. This might generally impact the ionic conduction in the porous electrodes as well as the polypropylene separator, which directly correlates to the cell performance at the cycling rates applied.^[39] Improvements were observed with sulfone electrolytes prepared with a higher ratio of EMC, where cells cycled with TMS/EMC (3/7) and EMS/EMC (3/7) maintained reversible discharge capacities of 95 mAhg⁻¹ and 86 mAhg⁻¹, respectively. When comparing the overall

coulombic efficiencies, the most significant improvement was observed in FEC and TMS-containing electrolytes, which reached values of 99.9% CE after 100 cycles. In contrast, cells cycled with EMS reached maximum CEs of 96.6% (3/7) and 99.4% (1/1), further indicating a less stable interphase layer formation in these electrolyte systems. Additional voltage profiles of LNMO||LTO cells cycled with all the electrolytes studied, along with corresponding differential capacity (dQ/dV) profiles and mean discharge potentials, are provided in the supporting information (Figures S4–S6). Generally, higher polarization, resulting in slightly lower discharge potentials and wider separation between the dQ/dV peaks during charge and discharge, was observed for FEC-based electrolytes compared to all sulfone-based electrolytes. This observation, despite the higher ionic conductivities of FEC-based electrolytes, suggests the formation of more resistive interphases on the electrodes in contact with FEC. Cells cycled with both TMS-based electrolytes and EMS/EMC 3/7 showed capacity fade without a noticeable drop in mean voltage. This data indicates Li inventory loss and incomplete cell discharge, likely due to depressed ionic conductivity and increased viscosity resulting from the decomposition of the EMC component.

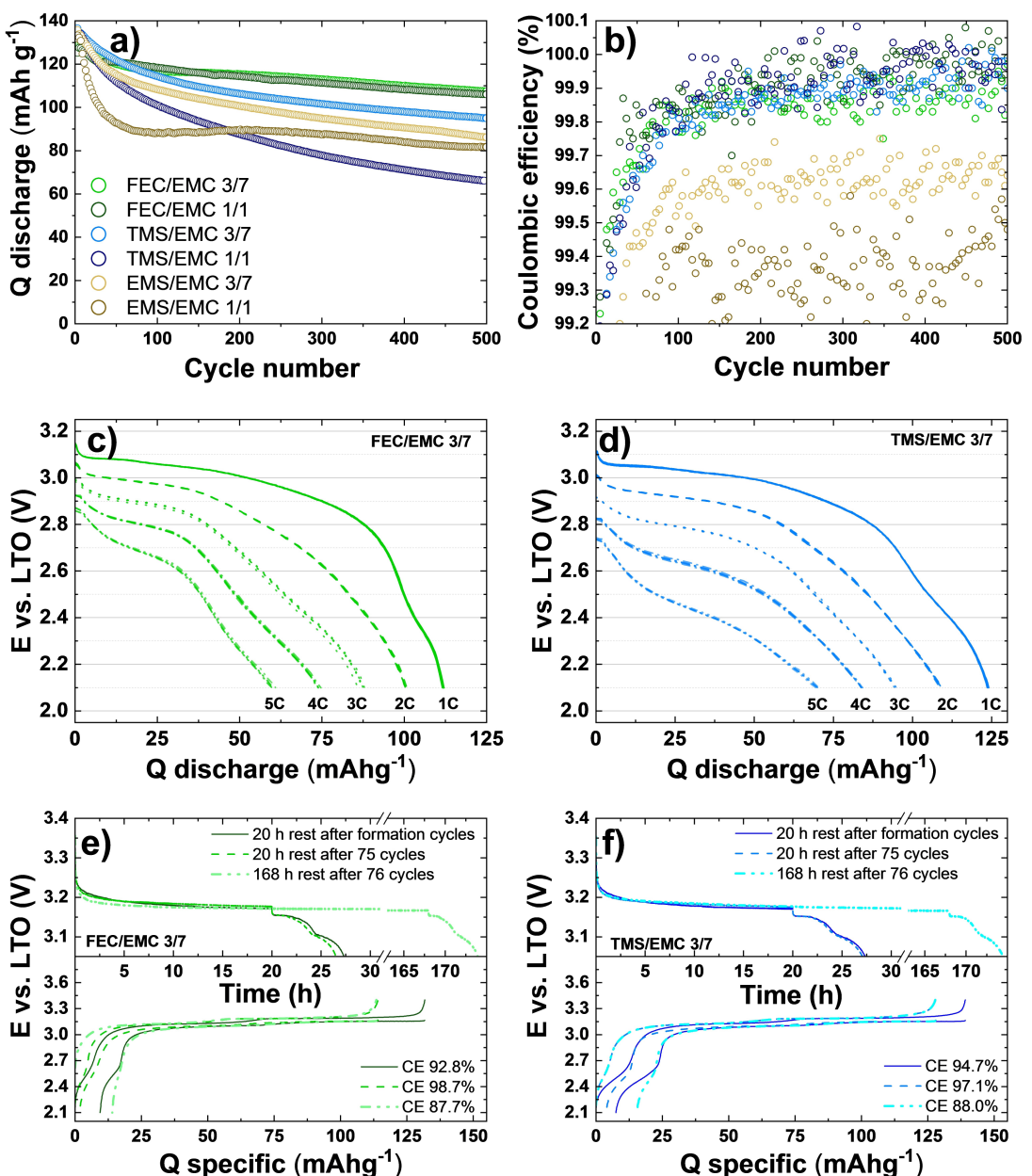


Figure 4. a) Charge and discharge capacities of the LNMO||LTO cells over 500 cycles when cycled in 1 M LiPF₆ salt dissolved in FEC/EMC (3/7), FEC/EMC (1/1), TMS/EMC (3/7), TMS/EMC (1/1), EMS/EMC (3/7) and EMS/EMC (1/1) electrolytes. b) Corresponding coulombic efficiency values, for the electrolytes, over 500 cycles. c and d) Rate acceptance test during discharge of FEC/EMC 3/7 and TMS/EMC based LNMO||LTO cells, and e) and f) self-discharge analysis after 20 h and 168 h rest for both electrolyte compositions.

The best-performing FEC and TMS electrolytes were further characterized for their rate acceptance. Figures 4c and 4d show the discharge voltage profiles at different C-rates, ranging from 1 C to 5 C, for LNMO||LTO cells with FEC/EMC (3/7) and TMS/EMC (3/7) electrolytes, respectively. The charge rate was kept constant at 0.5 C in all cases. Both electrolytes performed similarly at rates of 1–3 C. However, at higher rates, the TMS-based cell exhibited a more suppressed voltage, though it still achieved high capacities, likely due to the higher viscosity and lower ionic conductivity of the sulfone-based electrolyte.

Figure 4e and 4f examines the self-discharge behavior of LNMO||LTO cells using the FEC and the TMS-based electrolytes.

Cells were charged to 100% SoC and stored under OCV condition twice for 20 h and once for 7 days. In all cases, the cell potential quickly decayed to approximately 3.2 V before stabilizing. The first 20 h rest was performed directly after formation, and the second 20 h rest was implemented after 75 cycles when coulombic efficiencies had stabilized (>99.9%) (Figure 4b). The 7-day rest followed immediately after the second 20 h rest. As a measure for self-discharge, the coulombic efficiencies of the relevant cycles were compared. Both electrolytes exhibited similar behavior where, directly after formation, a reduced coulombic efficiency of 92.8% for the FEC-based electrolyte and 94.7% for the sulfolane-based electrolyte was

observed, indicating 7% and 5% self-discharge, respectively. After 75 cycles, the FEC-based cell lost approximately 1% of its capacity, while the sulfolane-based cell lost about 2.8% of its capacity. Both electrolytes showed significant self-discharge, of 12%, when stored charged for 7 days, suggesting continuous parasitic reactions.

High-resolution X-ray photoelectron spectroscopy (XPS) was employed to correlate electrode-specific interphase chemistry with electrochemical cell performance. We selected FEC/EMC (3/7) as the best performing overall electrolyte and TMS/EMC (3/7) as the best performing TMS-based electrolyte for this analysis. The chemical compositions of the LNMO cathode (CEI) and LTO anode (SEI) were analyzed after the cells were cycled 50 times, ensuring representative interphase layers had formed on the respective electrodes. Details on XPS sample preparation and test protocols are provided in the experimental section. The respective interphases were determined to be dominated by C, O, F, P containing species and, when TMS is used, S containing species as seen from the survey scans seen in supporting information (Figure S8).

Figure 5 presents the deconvoluted high-resolution spectra for C1s (Figure 5a), O1s (Figure 5b), F1s (Figure 5c), and P2p

(Figure 5d) for both the LNMO (CEI) (i, ii) and LTO (SEI) (iii, iv) electrodes cycled in FEC/EMC (green) and TMS/FEC (blue) electrolytes. The LNMO C1s spectra show characteristic signals from the underlying electrode, with a peak for carbon black at approximately 284.6 eV and a CF₂ peak related to the PVDF binder at 290.7 eV. Notably, the carbon black peak's relative intensity is lower for FEC/EMC compared to TMS, indicating a thicker CEI layer and more degradation products when FEC is used. This thicker CEI layer for FEC/EMC is corroborated by the lower intensity of the metal oxide (MO) signal (529.5 eV) in the LNMO O1s spectra compared to TMS/EMC.^[49,50] Conversely, the LTO C1s and O1s spectra reveal an opposite trend, with higher intensity signals for carbon black (C1s) and MO for FEC/EMC, indicating a thinner SEI layer compared to TMS/EMC. This suggests more extensive degradation of the TMS/EMC electrolyte on the anode side. Although TMS/EMC results in a more substantial SEI layer and FEC/EMC produces a denser CEI layer, the SEI remains significantly thicker than the CEI for both electrolytes. This suggests that the lower initial capacities and coulombic efficiencies for the FEC-containing electrolytes (Figure 3) represented more extensive interphase formation and

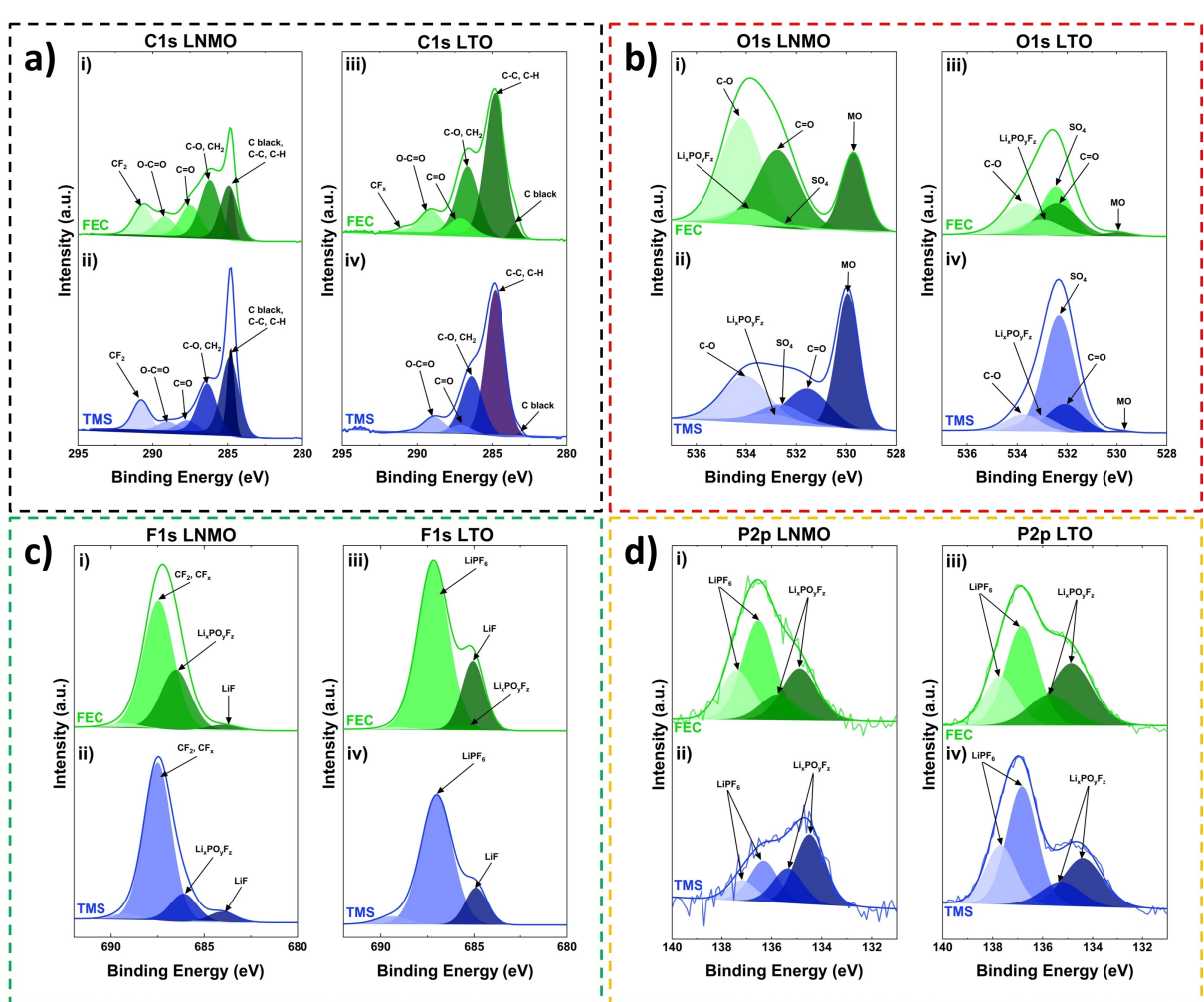


Figure 5. High resolution XPS a) C1s b) O1s, c) F1s and d) P2p spectra of the LNMO (i, ii) and LTO (iii, iv). Electrodes extracted from the cell after 50 cycles when cycled in either FEC/EMC 3/7 (green) or TMS/EMC 3/7 (blue) electrolyte.

subsequently yielded improved relative cycling performance (Figure 4a).

The C1s spectra for both electrolytes and electrodes reveal similar degradation species, including peaks for C–C/C–H (284.9 eV), C–O (286.5 eV), C=O (287.7 eV), and O–C=O (289.1 eV).^[51–54] For both the CEI and SEI the C–O contribution is the most prominent oxidized carbon species for all electrodes, indicating that these interphase layers are dominated by organic ether decomposition products rather than inorganic carbonates.^[27,55]

On the cathode side, there is almost identical intensities for the C=O and O–C=O/CO₃ peaks, while on the anode there is a higher O–C=O/CO₃ peak intensity than C=O. These observations are consistent with the O1s spectra, where the signals for C–O and C=O appear at binding energies around 533.5 eV and 532.5 eV, respectively.^[27,56] The low binding energy seen for deconvoluted C=O contribution for LNMO electrode with TMS electrolyte in Figure 4b ii) is erroneous and is a likely due to the omission of any hydroxide or defective oxide contribution in the fitting, where only the relative contributions from the other relevant regions (C 1s, S 2p, and P 2p) was considered. A notable difference in the LNMO O1s is the presence of an SO₄ signal for TMS/EMC, which is absent with FEC/EMC and likely originates from TMS decomposition. The presence of the SO₄ and other additional sulfur-containing species, is verified in the S2p spectra (supporting information, Figure S9), which are not observed with the FEC/EMC electrolyte. The high signal-to-noise ratio in the S2p spectrum for the TMS electrolyte suggests that sulfur-containing species form in low concentrations on the LNMO surface, indicating limited passivation of the cathode surface when TMS is present in the electrolyte. In contrast, the LTO S2p spectra show higher SO₄ intensity for both TMS and FEC electrolyte, whereas the additional species (e.g., SO₂–C doublet at 166.6 and 167.7 eV), are only present on the anode cycled with the TMS electrolyte.^[57,58] Caution should be taken as the commercial LTO anode contained sulfur-based species. SEM cross section and surface imaging together with an EDS point scan are presented in Figure S7 in the supporting information.

In the O1s spectra, a Li_xPO_yF_z peak is observed at approximately 533.9 eV, with corresponding signals detected in the F1s (686.5 eV) and P2p (doublet at 134.8 and 135.7 eV) spectra.^[10,28,29] This decomposition product is present in both the CEI and SEI for both electrolytes but at varying concentrations. The LNMO F1s spectra for FEC/EMC and TMS/EMC display a high intensity peak for CF₂/CF_x, primarily attributed to the PVDF binder, along with additional signals corresponding to LiF (684.8 eV) and Li_xPO_yF_z.^[31,59] Notably, the peak intensity of Li_xPO_yF_z is significantly higher for FEC/EMC than with TMS/EMC. Li_xPO_yF_z is known to effectively act as a transition metal scavenger, sequestering transition metals migrating from the cathode to the anode and mitigating parasitic side reactions between the electrolyte and the LNMO surface.^[10,60,61] Therefore, its presence in the interphase layers is beneficial and expected to bestow improvements during cell cycling. This correlates well with cycling performance observed in this study, where cells cycled in the FEC/EMC electrolyte display enhanced long-term cycling stability over counterparts cycled using the TMS/

EMC electrolyte. While appearing as a low intensity signal in the CEI, LiF appears to have a more substantial contribution to the composition of the SEI. A higher relative concentration of LiF on the LTO surface for FEC/EMC compared to TMS/EMC indicates a more LiF-rich interphase, generated by salt anion reduction. LiF has been shown to suppress solvent co-intercalation and improve long-term cycling stability, consistent with our galvanostatic cycling results.

To investigate the effect of electrolyte composition on transition metal migration from the cathode to the anode, we measured the Ti2p, Li1s, and Mn2p spectra, presented in Figure 6. Additionally, the high resolution XPS spectra of the Mn3 s–Mn3p region are available in the supporting information (Figure S10). The LTO Ti2p spectrum is dominated by a signal at 458.6 eV, corresponding to the binding energy for Ti 3/2 (TiO₂).^[62] This finding reinforces previous observations where the weaker TiO₂ signal for TMS/EMC suggests a thicker SEI layer on the LTO surface. In the Li1s spectrum, the most intense signal indicates the presence of LiF (55.8 eV), with a secondary peak attributed to contribution from the Mn3p (49.2 eV). The LTO Li1s spectrum shows a higher intensity Mn3p signal when TMS/EMC is used, compared to cells cycled in the FEC/EMC electrolyte. For LNMO Mn2p, the two characteristic 2p 1/2 and 2p 3/2 signals are observed, with lower intensity for FEC/EMC compared to TMS/EMC, confirming a thicker CEI formation when FEC is used. In Mn2p LTO, there is a clear disparity in peak intensities of the two Mn signals, indicating a higher concentration of Mn on the LTO surface with the TMS-containing electrolyte. A similar observation is made for Ni in Figure S10, where the higher peak intensity relating to Ni3p on the LTO SEI infers more extensive Ni migration when the TMS-based electrolyte is used. The higher concentration of Mn and Ni species on the anode side suggests that TMS is ineffective at passivating the LNMO surface and sequestering transition metal migration, relative to FEC. This is further evidenced by the lesser quantity of degradation products on the cathode and the reduced contribution of stabilizing species (Li_xPO_yF_z and LiF) on the interphases. These observations once again align closely with cycling performance data, where cells cycled with the FEC/EMC electrolyte improved long-term cycling stability and a lower amount of cross/talk between the anode and cathode.

Conclusions

In this study, we evaluated electrolytes comprising sulfones and fluorinated solvents for high voltage applications in LNMO||LTO cells. The alternative co-solvents were selected for their theoretically high oxidative stabilities as replacements for EC. Given the high viscosities of the sulfone solvents, we measured the ionic conductivity of all electrolytes as a function of temperature. While FEC-based electrolytes demonstrated ionic conductivities around 8 mS/cm, both sulfone-based electrolytes exhibited reduced ionic conductivities between 4–5 mS/cm, however, with lower temperature dependency. Analysis of the electrochemical stability of these co-solvents indicated a high anodic stability at room temperature which, is significantly

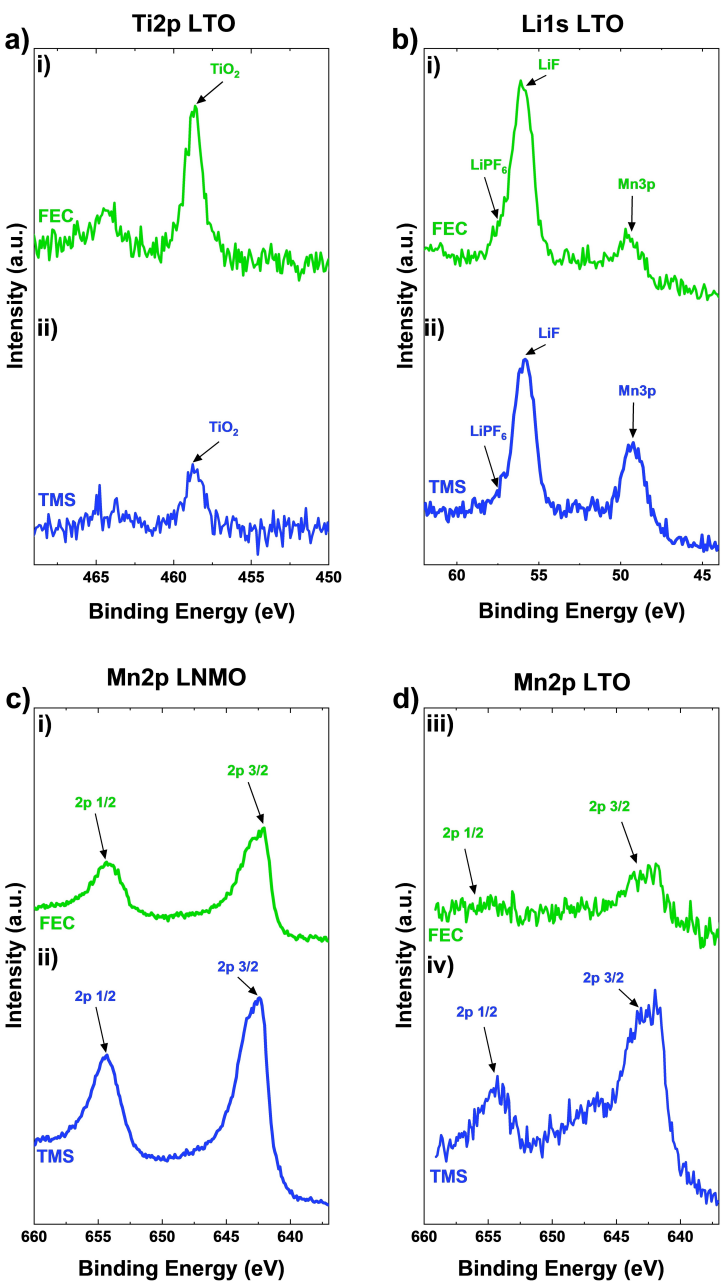


Figure 6. High resolution XPS a) Ti2p and b) Li1s spectra of the LTO (i, ii). High resolution XPS c) Mn2p spectra of the LNMO (i, ii) and LTO (iii, iv). Electrodes extracted from the cell after 50 cycles when cycled in either FEC/EMC 3/7 (green) or TMS/EMC 3/7 (blue) electrolyte.

reduced at elevated temperatures. These findings were supported by stable galvanostatic cycling at room temperature for several electrolyte formulations. While promising cycling stability was observed for: FEC/EMC (3/7), FEC/EMC (1/1), TMS/EMC (3/7), and EMS/EMC (3/7), the best performance was attained when FEC was used as a co-solvent where these cells retained approximately 85% of their capacity after 500 cycles. While these cells exhibited lower initial discharge capacities and coulombic efficiencies, this was likely due to the facilitation of a more extensive and stabilizing interphase layers. Post-mortem XPS analysis revealed differences in the SEI and CEI compositions. Cells cycled with FEC-containing electrolytes showed greater stabilization through the formation of higher concen-

trations of interphase species such as $\text{Li}_x\text{PO}_y\text{F}_z$ and LiF . In contrast, cycling with sulfone electrolytes resulted in thinner CEIs and thick, sulfur-rich SEIs that were observed to be insufficient in preventing transition metal dissolution and migration to the anode. Additionally, FEC-containing electrolytes showed significantly less transition metal migration from the LNMO cathode to the LTO anode, highlighting their potential as an alternative to EC. While further optimization, particularly of sulfone-based electrolytes with suitable additives, is required, these results represent significant progress toward realizing high voltage, enhanced energy density lithium-ion batteries that are EC-free.

Acknowledgements

The authors thank J.R. Tolchard for SEM-EDS analyses and A. Digranes for assistance with PEIS measurements. The research council of Norway is kindly acknowledged for funding of the strategic institute project Enerlyte through the basic grant received by SINTEF Industry. This work was performed within MoZEEs, a Norwegian Centre for Environment Friendly Energy Research (FME), co-sponsored by the Research Council of Norway (project number 257653) and 40 partners from research, industry and the public sector.

Conflict of Interests

The authors declare no conflict of interest.

Data Availability Statement

The data that support the findings of this study are available from the corresponding author upon reasonable request.

Keywords: LNMO · Li-ion · Ethylene carbonate free · Sulfone · Fluoroethylene carbonate

- [1] M. Kotal, S. Jakhar, S. Roy, H. K. Sharma, *J. Storage Mater.* **2022**, 47, 103534.
- [2] C. P. Grey, J. M. Tarascon, *Nature Mater.* **2017**, 16(1), 45–56.
- [3] K. Turcheniuk, D. Bondarev, G. G. Amatucci, G. Yushin, *Mater. Today* **2021**, 42, 57–72.
- [4] E. R. Østli, Y. Tesfamhret, S. Wenner, M. J. Lacey, D. Brandell, A. M. Svensson, S. M. Selbach, N. P. Wagner, *ACS Omega* **2021**, 6(45), 30644–30655.
- [5] J. Zhang, H. Zhang, S. Weng, R. Li, D. Lu, T. Deng, S. Zhang, L. Lv, J. Qi, X. Xiao, L. Fan, S. Geng, F. Wang, L. Chen, M. Noked, X. Wang, X. Fan, *Nat Commun* **2023**, 14(1), 2211.
- [6] J. Alvarado, M. A. Schroeder, M. Zhang, O. Borodin, E. Gobrogue, M. Olguin, M. S. Ding, M. Gobet, S. Greenbaum, Y. S. Meng, K. A. C.-F. Xu, *Mater. Today* **2018**, 21(4), 341–353.
- [7] P. Arora, R. E. White, M. Doyle, *J. Electrochem. Soc.* **1998**, 145(10), 3647.
- [8] L. Xing, W. Li, C. Wang, F. Gu, M. Xu, C. Tan, J. Yi, *J. Phys. Chem. B* **2009**, 113(52), 16596–16602.
- [9] M. Metzger, B. Strehle, S. Solchenbach, H. A. Gasteiger, *J. Electrochem. Soc.* **2016**, 163(5), A798.
- [10] S. Klein, S. van Wickeren, S. Röser, P. Bärmann, K. Borzutzki, B. Heidrich, M. Börner, M. Winter, T. Placke, J. Kasnatscheew, *Adv. Energy Mater.* **2021**, 11(14), 2003738.
- [11] S. Klein, P. Harte, S. van Wickeren, K. Borzutzki, S. Röser, P. Bärmann, S. Nowak, M. Winter, T. Placke, J. Kasnatscheew, *Cell Reports Physical Science* **2021**, 2(8), 100521.
- [12] S. Klein, L. Haneke, P. Harte, L. Stoltz, S. van Wickeren, K. Borzutzki, S. Nowak, M. Winter, T. Placke, J. Kasnatscheew, *ChemElectroChem* **2022**, 9(13), e202200469.
- [13] X. Sun, C. A. Angell, *Electrochem. Commun.* **2009**, 11(7), 1418–1421.
- [14] S.-Y. Lee, K. Ueno, C. A. Angell, *J. Phys. Chem. C* **2012**, 116(45), 23915–23920.
- [15] L. Xue, K. Ueno, S.-Y. Lee, C. A. Angell, *J. Power Sources* **2014**, 262, 123–128.
- [16] K. Xu, C. A. Angell, *J. Electrochem. Soc.* **2002**, 149(8), L7.
- [17] K. Xu, A. Cresce, *J. Mater. Chem.* **2011**, 21(27), 9849–9864.
- [18] V. Etacheri, O. Haik, Y. Goffer, G. A. Roberts, I. C. Stefan, R. Fasching, D. Aurbach, *Langmuir* **2012**, 28(1), 965–976.
- [19] Z. L. Brown, S. Jurng, C. C. Nguyen, B. L. Lucht, *ACS Appl. Energy Mater.* **2018**, 1(7), 3057–3062.
- [20] Y. Kang, J. Wang, M. Wang, X. Tang, Z. Cao, C. Wang, Q. Shi, Y. Qian, Y. Deng, *Energy Mater.* **2020**, 3(10), 9989–10000.
- [21] J. Yang, Q. Liu, K. Z. Pupek, T. L. Dzwiniel, N. L. Dietz Rago, J. Cao, N. Dandu, L. Curtiss, K. Liu, C. Liao, Z. Zhang, *ACS Energy Lett.* **2021**, 6(2), 371–378.
- [22] Z. Hu, L. Zhao, T. Jiang, J. Liu, A. Rashid, P. Sun, G. Wang, C. Yan, L. Zhang, *Adv. Funct. Mater.* **2019**, 29(45), 1906548.
- [23] J. Im, J. Lee, M.-H. Ryou, Y. M. Lee, K. Y. Cho, *J. Electrochem. Soc.* **2017**, 164(1), A6381–A6385.
- [24] C.-C. Su, M. He, R. Amine, T. Rojas, L. Cheng, A. T. Ngo, K. Amine, *Energy Environ. Sci.* **2019**, 12(4), 1249–1254.
- [25] C.-C. Su, M. He, M. Cai, J. Shi, R. Amine, N. D. Rago, J. Guo, T. Rojas, A. T. Ngo, K. Amine, *Nano Energy* **2022**, 92, 106720.
- [26] Q. Li, J. Chen, L. Fan, X. Kong, Y. Lu, *Green Energy Environ.* **2016**, 1(1), 18–42.
- [27] B. Aktekin, R. Younesi, W. Zipprich, C. Tengstedt, D. Brandell, K. Edström, *J. Electrochem. Soc.* **2017**, 164(4), A942.
- [28] E. Markevich, G. Salitra, D. Aurbach, *ACS Energy Lett.* **2017**, 2(6), 1337–1345.
- [29] V. Tarnopolskiy, J. Kalhoff, M. Nádherná, D. Bresser, L. Picard, F. Fabre, M. Rey, S. Passerini, *J. Power Sources* **2013**, 236, 39–46.
- [30] H. Shin, J. Park, A. M. Sastry, W. Lu, *J. Electrochem. Soc.* **2015**, 162(9), A1683.
- [31] M.-H. Ryou, G.-B. Han, Y. M. Lee, J.-N. Lee, D. J. Lee, Y. O. Yoon, J.-K. Park, *Electrochim. Acta* **2010**, 55(6), 2073–2077.
- [32] Y.-B. He, B. Li, M. Liu, C. Zhang, W. Lv, C. Yang, J. Li, H. Du, B. Zhang, Q.-H. Yang, J.-K. Kim, F. Kang, *Sci Rep* **2012**, 2(1), 913.
- [33] W. Cui, Y.-B. He, Z.-Y. Tang, Q.-H. Yang, Q. Xu, F.-Y. Su, L. Ma, *J. Solid State Electrochem* **2012**, 16(1), 265–271.
- [34] M. S. Ding, K. Xu, T. R. Jow, *J. Electrochem. Soc.* **2000**, 147(5), 1688.
- [35] J. Barthel, H. J. Gores Liquid Nonaqueous Electrolytes. In *Handbook of Battery Materials*, John Wiley & Sons, Ltd **1998**, pp. 457–497.
- [36] N. Shao, X.-G. Sun, S. Dai, D. Jiang, *J. Phys. Chem. B* **2011**, 115(42), 12120–12125.
- [37] Y. Hayashi, M. Sohmiya, H. Otsuka, K. Ito, Y. Kubo, T. Horiba, M. Saito, *J. Electrochem. Soc.* **2020**, 167(16), 160531.
- [38] M. Kobayashi, T. Inoguchi, T. Iida, T. Tanioka, H. Kumase, Y. Fukai, *J. Fluorine Chem.* **2003**, 120(2), 105–110.
- [39] A. Abouimrane, I. Belharouak, K. Amine, *Electrochem. Commun.* **2009**, 11(5), 1073–1076.
- [40] H. Vogel, *Physikalische Zeitschrift* **1921**, 22, 245–257.
- [41] G. S. Fulcher, *J. Am. Ceram. Soc.* **1925**, 8(6), 339–355.
- [42] G. Tammann, W. Hesse, *Zeitschrift für anorganische und allgemeine Chemie* **1926**, 156(1), 245–257.
- [43] J. Landesfeind, H. A. Gasteiger, *J. Electrochem. Soc.* **2019**, 166(14), A3079.
- [44] P. Hilbig, L. Ibing, R. Wagner, M. Winter, I. Cekic-Laskovic, *Energies* **2017**, 10(9), 1312.
- [45] B. Aktekin, M. Valvo, R. I. Smith, M. H. Sørby, F. Lodi Marzano, W. Zipprich, D. Brandell, K. Edström, W. R. Brant, *Energy Mater.* **2019**, 2(5), 3323–3335.
- [46] J. Xia, R. Petibon, D. Xiong, L. Ma, J. R. Dahn, *J. Power Sources* **2016**, 328, 124–135.
- [47] T. Hou, G. Yang, N. N. Rajput, J. Self, S.-W. Park, J. Nanda, K. A. Persson, *Nano Energy* **2019**, 64, 103881.
- [48] K. Yao, J. P. Zheng, R. Liang, *J. Power Sources* **2018**, 381, 164–170.
- [49] K. Edström, T. Gustafsson, J. O. Thomas, *Electrochim. Acta* **2004**, 50(2–3), 397–403.
- [50] H. N. Pollen, I.-E. Nylund, Dahl, A. M. Svensson, D. Brandell, R. Younesi, J. R. Tolchard, N. P. Wagner, *Energy Mater.* **2023**.
- [51] E. Björklund, D. Brandell, M. Hahlin, K. Edström, R. Younesi, *J. Electrochem. Soc.* **2017**, 164(13), A3054.
- [52] J.-B. Gieu, V. Winkler, C. Courrèges, L. E. Ouatani, C. Tessier, H. Martinez, *J. Mater. Chem. A* **2017**, 5(29), 15315–15325.
- [53] N. Gauthier, C. Courrèges, J. Demeaux, C. Tessier, H. Martinez, *Appl. Surf. Sci.* **2020**, 501, 144266.
- [54] S. Malmgren, K. Ciosek, M. Hahlin, T. Gustafsson, M. Gorgoi, H. Rensmo, K. Edström, *Electrochim. Acta* **2013**, 97, 23–32.
- [55] H. Jia, Y. Xu, L. Zou, P. Gao, X. Zhang, B. Taing, B. E. Matthews, M. H. Engelhard, S. D. Burton, K. S. Han, L. Zhong, C. Wang, W. Xu, *J. Power Sources* **2022**, 527, 231171.
- [56] E. R. Østli, A. Mathew, J. R. Tolchard, D. Brandell, A. M. Svensson, S. M. Selbach, N. P. Wagner, *Batteries & Supercaps* **2023**, 6(7), e202300085.
- [57] Table of Elements - NO. <https://www.thermofisher.com/uk/en/home/materials-science/learning-center/periodic-table.html>.(accessed 2024-06-04)..

- [58] Q. Zheng, G. Li, X. Zheng, L. Xing, K. Xu, W. Li, *Energy Environ. Mater.* **2022**, *5*(3), 906–911.
- [59] J. Demeaux, E. D. Vito, D. Lemordant, M. L. Digabel, H. Galiano, M. Caillon-Caravanier, B. Claude-Montigny, *Phys. Chem. Chem. Phys.* **2013**, *15*(48), 20900–20910.
- [60] S. Klein, K. Borzutzki, P. Schneider, O. Fromm, J. Reiter, Q. Fan, T. Placke, M. Winter, J. Kasnatscheew, *Chem. Mater.* **2020**, *32*(15), 6279–6284.
- [61] L. Xia, B. Tang, L. Yao, K. Wang, A. Cheris, Y. Pan, S. Lee, Y. Xia, G. Z. Chen, Z. Liu, *ChemistrySelect* **2017**, *2*(24), 7353–7361.
- [62] R. Dedryvère, D. Foix, S. Franger, S. Patoux, L. Daniel, D. Gonbeau, *J. Phys. Chem. C* **2010**, *114*(24), 10999–11008..

Manuscript received: July 4, 2024
Revised manuscript received: August 15, 2024
Accepted manuscript online: August 29, 2024
Version of record online: October 23, 2024
